WAVE PROPAGATION AND LOCALIZATION IN A RATE-DEPENDENT CRACKED MEDIUM—MODEL FORMULATION AND ONE-DIMENSIONAL EXAMPLES

L. J. SLUYS

Delft University of Technology, Department of Civil Engineering, P.O. Box 5048,
2600 GA Delft, Netherlands

and

R. DE BORST

Delft University of Technology, Department of Civil Engineering, TNO Building and Construction
Research, P.O. Box 5048, 2600 GA Delft, Netherlands

Abstract—A smeared-crack model is proposed in which the stress after cracking is not only a function of the crack strain (softening function), but also of the crack strain rate. This rate dependence is shown to introduce an internal length scale into initial value problems. As a result, solutions of initial value problems that involve smeared cracking remain well posed. The width of the localization zone, where high strain rates are present, is proven to be independent of the finite element discretization. Convergence upon mesh refinement is also obtained for the consumption of energy in a cracked bar and the extent of wave reflection on a cracked zone. This is because in a rate-dependent medium, waves are dispersive and propagate with a real wave speed. Numerical results have been obtained for one-dimensional localization problems to substantiate these analytical findings.

1. INTRODUCTION

To carry out failure analyses of concrete structures, which are subjected to transient loading conditions, it is important to properly model cracking. In a structural concrete member micro-cracking leads to a local reduction in the effective cross-sectional area that transmits tensile forces. This phenomenon is commonly called softening and is accompanied by the formation of narrow bands of intense straining (localization of deformation). This softening behaviour is measured in experiments and the mapping of thus obtained load–displacement data onto stress–strain relations leads to a negative slope in the stress–strain curve.

Analytical solutions of transient problems that involve softening (Bažant and Belytschko, 1985) show localization zones of zero thickness with infinite strains (line cracks) which develop in a period of time that approaches zero. Numerical simulations of a softening solid exhibit the same features upon mesh refinement (Sluys, 1989). The finite element solution tries to capture the line crack and, as a result, strain localization occurs in the smallest possible zone that is allowed by the discretization. For one-dimensional constant strain elements the smallest possible zone is one element wide. Upon mesh refinement the element size goes to zero and the analytical solution is therefore approached in an asymptotic sense. Furthermore, the energy dissipation in the fracture zone tends to zero upon mesh refinement and the extent of wave reflection on cracks depends on the discretization of a structure. Finally, the direction of crack propagation is influenced by the orientation of the mesh lines and does not comply with the direction predicted analytically by linear stability analyses in the sense of Rudnicki and Rice (1975). This observation is closely related to the issue of mesh refinement versus mesh alignment. Indeed, numerical studies (Sluys, 1992) show that, even if the energy dissipation is kept constant, e.g. by using a crack band model (Bažant and Oh, 1983), there remains a mesh dependence with respect to the direction of propagation.

Three types of methods have been suggested in the literature to correct the above-mentioned deficiencies. These so-called regularization methods are based on the introduction of additional terms in the continuum description. The first class of methods consists of non-local models (Pijaudier-Cabot and Bažant, 1987) and gradient models (de Borst and Mühlhaus, 1991a,b; Lasry and Belytschko, 1988; Mühlhaus and Aifantis, 1991; Schreyer and Chen, 1986; Sluys *et al.*, 1991) in which higher-order displacement gradients are introduced in the material equations. A second approach is the micro-polar (Cosserat) theory which allows mesh-objective analyses to be carried out under mode-II and mixed-mode conditions. This holds true for static (de Borst, 1990; de Borst and Mühlhaus, 1991a; Mühlhaus *et al.*, 1991) as well as dynamic loading conditions (de Borst and Sluys, 1991). The third solution strategy, followed in this article, is based on the inclusion of the strain rate in the constitutive equations (Needleman, 1988; Sluys and de Borst, 1991; Wu and Freund, 1984). The models have in common, firstly, that an internal length scale is incorporated and, secondly, that under transient loading conditions wave propagation is dispersive.

Rate dependence is introduced to prevent the character of the set of equations that describes the dynamic motion of the softening solid from becoming elliptic. In dynamics equations should possess real characteristics in the x–t plane which is only possible if the initial value problem is not elliptic. Then, well-posedness of the initial value problem is preserved and meaningful results can be obtained for localized zones of intense straining. Because failure modes are usually accompanied by high strain rates the inclusion of the strain rate in the constitutive equations seems natural. It is essential for the solution of the mesh-sensitivity problem that rate dependence naturally introduces an internal length scale into the initial value problem, although the constitutive equations do not explicitly contain a parameter with the dimension of length.

This paper will start by extending the crack model of de Borst and Nauta (1985) to include rate effects. Next, the algorithmic aspects are discussed that are necessary for numerical applications. The existence of the length scale is proven from an analysis of dispersive waves and the model is compared with other rate-dependent models (Loret and Prevost, 1990; Needleman, 1988; Perzyna, 1966; Simo *et al.*, 1988). Finally numerical analyses are included to assess the performance of the model with respect to mesh refinement.

The prime aim of this study is not the exact simulation of the experimentally measured response, rather it is the purpose to model the softening solid properly in a mathematical sense. The rate-dependent crack model is still in a developing stage and tuning of the results to experimental data has been done but not extensively. An example is the simulation of an impact tensile test on a double-notched specimen, in which similarity between experimental and numerical results has been obtained (Sluys and de Borst, 1992). In non-classical formulations of the strain-softening solid the additional parameters are not directly derivable from experiments and therefore the semi-inverse approach for the determination of the internal length scale parameter is followed in the latter contribution. In fact, a direct determination of the material parameters is not possible when softening models are used within the classical continuum approach. This has been demonstrated by Rots and de Borst (1989) when analysing the behaviour of a statically loaded, double-notched specimen with the aid of a classical, rate-independent smeared-crack model.

2. FORMULATION OF A RATE-DEPENDENT CRACK MODEL

A crack model that exhibits both softening and strain rate dependence is chosen according to

$$\sigma = f(\varepsilon_{cr}) + m\dot{\varepsilon}_{cr}, \tag{1}$$

where σ and ε_{cr} denote stress and crack strain respectively, a superimposed dot denotes differentiation with respect to time, $f(\varepsilon_{cr})$ is a softening function and m is the rate-sensitivity

parameter. Note that rate dependence is chosen as a function of the crack strain ε_{cr} and not of the total strain. When a linear softening function is utilized as in this study:

$$f(\varepsilon_{cr}) = f_t + h\varepsilon_{cr},\tag{2}$$

eqn (1) becomes

$$\sigma = f_t + h\varepsilon_{cr} + m\dot{\varepsilon}_{cr}.\tag{3}$$

In eqns (2) and (3) f_t is the initial tensile strength under static loading conditions and h is a constant softening modulus. For unloading a secant modulus without rate dependence is used. In the reference calculations the parameters have been chosen as: Young's modulus $E = 20\,000$ N mm^{-2}, $h = -5000$ N mm^{-2}, $m = 0.2$ N s mm^{-2} (which corresponds to a relaxation time $\eta = 1 \cdot 10^{-5}$ s) and $f_t = 2.0$ N mm^{-2}.

In Fig. 1 the computed stress–strain curves are shown for various imposed strain rates. The curves show an increase of the tensile strength (σ/f_t) under dynamic loading, which is also observed in several experiments (Körmeling, 1986; Zielinski, 1982). In these experiments the increase of tensile strength is measured as a function of a constant strain rate. However, these test series and the numerical simulations described in the subsequent section show that the strain rate not only varies in time but also displays large gradients along the localization zone. It is therefore difficult to derive the material rate sensitivity parameter m from experimental data and semi-inverse modelling techniques are necessary. As regards the increase of fracture energy per unit area and the ultimate strain less experimental support currently exists, although Körmeling (1986) observed the same tendencies in softening behaviour under high strain rates.

The rate-dependent crack model has been implemented within the framework of the fixed smeared crack concept (de Borst and Nauta, 1985; Rots, 1988). In this concept a cracked zone is conceived to be a continuum which permits a description in terms of stress–strain relations. We apply a decomposition of total strain rate into the elastic strain rate $\dot{\varepsilon}_e$ and the crack strain rate $\dot{\varepsilon}_{cr}$:

$$\dot{\varepsilon} = \dot{\varepsilon}_e + \dot{\varepsilon}_{cr}.\tag{4}$$

The stress–strain relation can be written in a rate form as

$$\dot{\sigma} = D_e(\dot{\varepsilon} - \dot{\varepsilon}_{cr}),\tag{5}$$

where the matrix D_e contains the instantaneous moduli of the concrete. After a generalization of eqn (3) to two dimensions we obtain
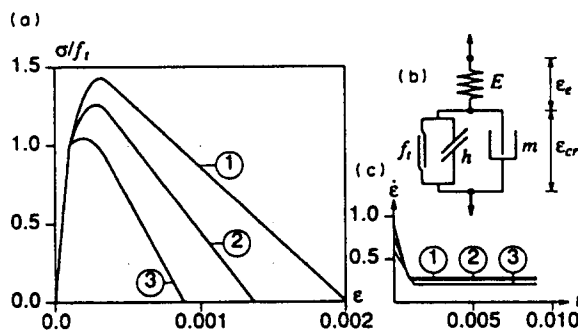

Fig. 1. Rate-dependent crack model. (a) Stress–strain curves for different imposed strain rates. (b) Schematic representation of the model. (c) Imposed strain rates.

$$\dot{\sigma} = D_{cr}\dot{\varepsilon}_{cr} + M\ddot{\varepsilon}_{cr}. \tag{6}$$

in which $D_{cr} = \text{diag}[h, 0]$ and $M = \text{diag}[m, 0]$, so that only mode-I effects are considered. Combination of eqns (5) and (6) yields

$$\dot{\varepsilon}_{cr} = (D_e + D_{cr})^{-1}[D_e\dot{\varepsilon} - M\ddot{\varepsilon}_{cr}]. \tag{7}$$

This equation can be substituted into eqn (5), which gives the global constitutive equation:

$$\dot{\sigma} = D_e[I - (D_e + D_{cr})^{-1}D_e]\dot{\varepsilon} + D_e[D_e + D_{cr}]^{-1}M\ddot{\varepsilon}_{cr}. \tag{8}$$

For the sake of simplicity only one crack has been considered in this derivation and the axes of the crack plane are assumed to be aligned with the global element axes. For a general treatment of the rate-dependent smeared-crack model see Sluys and de Borst (1992) and Sluys (1992).

3. ALGORITHMIC ASPECTS

Using the rate equations for the rate-dependent crack model we can develop an algorithm that determines the stress increment in a finite time step Δt. Therefore we consider the stress–strain eqn (5) in its incremental form

$$\Delta\sigma = D_e(\Delta\varepsilon - \Delta\varepsilon_{cr}), \tag{9}$$

in which we define $\Delta\sigma$, $\Delta\varepsilon$ and $\Delta\varepsilon_{cr}$ as the increments in a time interval $t \leqslant \tau \leqslant t + \Delta t$. Denoting the crack strain rate at the beginning of the time step by $\dot{\varepsilon}_{cr}^t$ and at the end of the time step by $\dot{\varepsilon}_{cr}^{t+\Delta t}$, the incremental crack strain is chosen according to

$$\Delta\varepsilon_{cr} = ((1-\Theta)\dot{\varepsilon}_{cr}^t + \Theta\dot{\varepsilon}_{cr}^{t+\Delta t})\Delta t, \tag{10}$$

where Θ is an interpolation parameter, $0 \leqslant \Theta \leqslant 1$. For $\Theta = 0$ we obtain the fully explicit Euler scheme. On the other hand $\Theta = 1$ gives a scheme that is fully implicit and the case in which $\Theta = \frac{1}{2}$ represents an implicit scheme according to the trapezoidal rule. At the beginning of the time interval the crack strain rate reads

$$\dot{\varepsilon}_{cr}^t = [M]^{-1}(\sigma^t - \sigma_{cr}^t), \tag{11}$$

in which $\sigma_{cr}^t = D_{cr}\varepsilon_{cr}^t$. The crack strain rate at the end of the time interval is expressed in a limited Taylor series expansion as

$$\dot{\varepsilon}_{cr}^{t+\Delta t} = \dot{\varepsilon}_{cr}^t + \left(\frac{\partial\dot{\varepsilon}_{cr}}{\partial\sigma}\right)^t\Delta\sigma + \left(\frac{\partial\dot{\varepsilon}_{cr}}{\partial\sigma_{cr}}\right)^t\left(\frac{\partial\sigma_{cr}}{\partial\varepsilon_{cr}}\right)^t\Delta\varepsilon_{cr}, \tag{12}$$

which can be rewritten as

$$\dot{\varepsilon}_{cr}^{t+\Delta t} = \dot{\varepsilon}_{cr}^t + [M]^{-1}(\Delta\sigma - D_{cr}\Delta\varepsilon_{cr}). \tag{13}$$

By combination of eqns (9), (10) and (13) we obtain an explicit relation for the incremental crack strain:

$$\Delta\varepsilon_{cr} = (D_e + D_{cr} + (1/(\Theta\Delta t))M)^{-1}[D_e\Delta\varepsilon + (1/\Theta)M\dot{\varepsilon}_{cr}^t]. \tag{14}$$

This equation can be substituted into eqn (9) to obtain the incremental constitutive relation at time $t + \Delta t$:

$$\Delta\sigma = \mathbf{D}_{\text{tan}}\Delta\varepsilon - \Delta\mathbf{q}. \tag{15}$$

where

$$\mathbf{D}_{\text{tan}} = \mathbf{D}_{\text{e}}[\mathbf{I} - (\mathbf{D}_{\text{e}} + \mathbf{D}_{\text{cr}} + (1/(\Theta\Delta t))\mathbf{M})^{-1}\mathbf{D}_{\text{e}}] \tag{16}$$

and

$$\Delta\mathbf{q} = (1/\Theta)\mathbf{D}_{\text{e}}[\mathbf{D}_{\text{e}} + \mathbf{D}_{\text{cr}} + (1/(\Theta\Delta t))\mathbf{M}]^{-1}\mathbf{M}\dot{\varepsilon}'_{\text{cr}}. \tag{17}$$

Matrix $\mathbf{D}_{\text{tan}}$ is determined not only by material parameters since the time integration parameters Δt and Θ also enter the expression. The vector $\Delta\mathbf{q}$ can be considered as a pseudo-load and a pseudo-nodal force vector can be deduced according to

$$\Delta\mathbf{f}_{\text{rd}} = \int_{\Gamma} \mathbf{B}^{\text{T}}\Delta\mathbf{q}\, d\Gamma. \tag{18}$$

in which $\mathbf{B}^{\text{T}}$ is the strain–nodal displacement matrix. The pseudo-nodal force vector is included in the discretized equations of motion. For the solution of the non-linear set of algebraic equations we use the iterative Newton–Raphson method.

4. WAVE PROPAGATION IN A RATE-DEPENDENT BAR

We investigate wave propagation by considering the set of equations for a one-dimensional bar. The constitutive equation is given in (3) and the equation of motion and the kinematic equation read

$$\frac{\partial\sigma}{\partial x} = \rho\frac{\partial^2 u}{\partial t^2} \tag{19}$$

and

$$\varepsilon = \frac{\partial u}{\partial x}. \tag{20}$$

with ρ density and t denoting time. Combining eqns (3), (19) and (20) with eqn (4) and taking $\varepsilon_{\text{e}} = \sigma/E$ with E the Young's modulus, we obtain the third-order differential equation

$$m\left(\frac{1}{c_{\text{e}}^2}\frac{\partial^3 u}{\partial t^3} - \frac{\partial^3 u}{\partial x^2 \partial t}\right) + \frac{E+h}{c_{\text{e}}^2}\frac{\partial^2 u}{\partial t^2} - h\frac{\partial^2 u}{\partial x^2} = 0. \tag{21}$$

By considering the third-order terms in eqn (21) the wave equation for the rate-dependent, strain-softening bar has real characteristics, which are equal to the linear elastic wave velocity $\pm c_{\text{e}}(=\sqrt{E/\rho})$. This means that the wave equation remains hyperbolic and the initial value problem is well posed. However, the characteristics no longer equal the physical wave speed in the rate-dependent bar. This is only the case if the second-order terms in eqn (21) are absent ($m \to \infty$) and the wave speed exactly equals the elastic wave velocity c_{e}. So, the suggestions in literature (Loret and Prevost, 1990; Needleman, 1988) that in a rate-dependent continuum disturbances due to inelastic effects travel with the elastic wave speed are correct for the limiting case. The last two terms in eqn (21) are the same as in the rate-independent problem ($m = 0$). In the latter case, i.e. in a conventional continuum, the wave speed c can be expressed as

$$c = c_{\text{e}}\left(\frac{h}{E+h}\right)^{1/2}. \tag{22}$$

It is obvious that the wave speed becomes imaginary and consequently provides physically

meaningless results as soon as softening occurs ($h < 0$). An imaginary wave speed corresponds to a standing wave which does not have the ability to extend the localization zone.

Now, the dispersive character of wave propagation in our rate-dependent, softening continuum will be investigated. To this end a general solution for a single linear harmonic wave propagating through the bar is assumed to be of the form

$$u(x, t) = A\, e^{i(kx - \omega t)},$$ (23)

in which ω is the angular frequency and k is the wave number counting the number of wave lengths L in the bar over 2π:

$$k = \frac{2\pi}{L}.$$ (24)

The waves are called dispersive if the phase velocity $c_f = \omega/k$ is a function of k, while the waves are non-dispersive if c_f is independent of k, which is the case for a rate-independent continuum. In a dispersive medium a distinction may exist between the phase velocity c_f of the single harmonic wave and the group velocity $c_g = \partial\omega/\partial k$ which is the velocity at which the energy travels. The dispersion relation in a non-explicit notation can be obtained by substitution of eqn (23) into eqn (21)

$$(\rho m \omega^3 - mEk^2\omega)i - \rho(E + h)\omega^2 + hEk^2 = 0.$$ (25)

If we consider ω and k to be real no solution is possible. Equation (25) can only be satisfied if k is complex and therefore k is set to be equal to $k_r + \alpha i$. This complex value for k means that the harmonic wave is attenuated exponentially as it proceeds through the solid and the expression for $u(x, t)$ may now be written as

$$u(x, t) = A\, e^{-\alpha x}\, e^{i(k_r x - \omega t)}.$$ (26)

If we equate real and imaginary parts of eqn (25) we obtain, respectively,

$$k_r^2 = \frac{\rho\omega^2}{2E}\left(\frac{-(m^2\omega^2 + h^2 + Eh) + ((m^2\omega^2 + h^2 + Eh)^2 + (mE\omega)^2)^{1/2}}{m^2\omega^2 + h^2}\right)$$ (27)

and

$$\alpha^2 = \frac{\rho\omega^2}{2E}\left(\frac{+(m^2\omega^2 + h^2 + Eh) + ((m^2\omega^2 + h^2 + Eh)^2 + (mE\omega)^2)^{1/2}}{m^2\omega^2 + h^2}\right).$$ (28)

In Fig. 2 the results for the dispersive wave propagation are plotted for the reference parameter set. In the upper figure the dispersion relation $\omega = f(k_r)$ shows that waves in a rate-dependent softening continuum behave similarly to waves in a linear elastic continuum. If k_r approaches zero, i.e. for waves of a very low frequency (i.e. a static response), the slope of the dispersion curve becomes infinite for softening ($h < 0$) whereas it vanishes for hardening and perfect plasticity ($h \geqslant 0$). In the centre graph of Fig. 2 the phase velocity $c_f = \omega/k_r$ is plotted. In the rate-dependent, strain-softening bar wave propagation is dispersive because the phase velocity is a function of k_r and ω. The dispersion property implies that the rate-dependent strain-softening continuum is able to transform the shape of travelling waves because the harmonic components have mutually different phase velocities. In localization analyses this has the advantageous effect that arbitrarily shaped waves can be transformed in the localization zone. The group velocity $c_g = \partial\omega/\partial k_r$, also plotted in the centre graph of Fig. 2, becomes infinite for $\omega \to 0$. In this case the damper element plays no role any more and a non-physical situation arises in which the energy
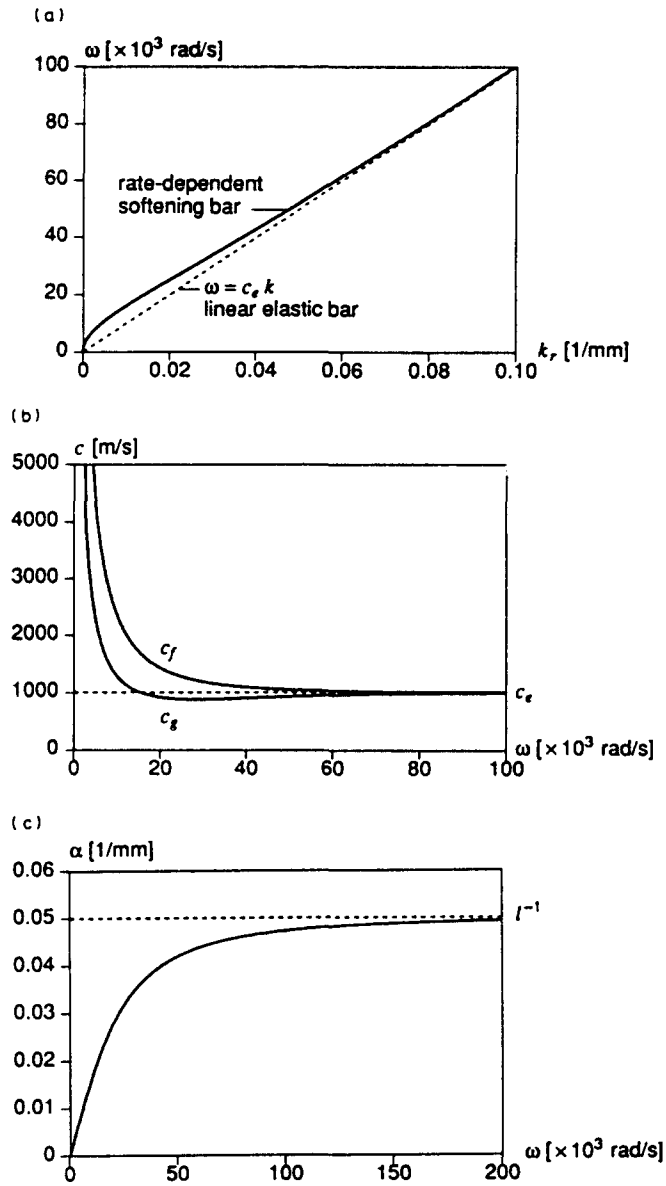
Fig. 2. Wave propagation behaviour for a rate-dependent bar. (a) Dispersion relation. (b) Phase and group velocity as a function of ω. (c) Damping coefficient α as a function of ω.

travels with an infinite velocity. Thus for very low frequencies, i.e. a static response, the regularization effect by the viscous terms vanishes. For higher frequencies a positive wave speed is obtained which approaches the linear elastic velocity c_e. For the consideration of localization problems this positiveness of the wave speed is essential. In the bottom curve of Fig. 2 the damping coefficient α is plotted as a function of ω according to eqn (28). The limit of α with respect to ω reads

$$\lim_{\omega \to \infty} \alpha(\omega) = l^{-1}, \quad \text{with} \quad l = \frac{2mc_e}{E}. \tag{29}$$

The parameter l is the internal length scale of this rate-dependent crack model. High frequencies are attenuated exponentially in the space domain to an extent which is determined by the length scale l. The implicit presence of an internal length scale is therefore essential.

A complete analytical solution of a softening rate-dependent bar is not known and the analytical treatment here is limited to the derivation of the dispersion relationships for a single mode. For the total solution of a one-dimensional bar problem we have to rely entirely on numerical techniques.

5. RELATION TO OTHER RATE-DEPENDENT MODELS

Rate effects not only play an important role during fracture processes but also during plastic deformation. Hence in the visco-plasticity theory rate dependence is also included in the material description. For the visco-plastic modelling two main approaches are available, namely the Perzyna theory and the Duvaut–Lions theory. In the theory proposed by Perzyna (1966) the plastic strain rate $\dot{\varepsilon}_{pl}$ is defined as

$$\dot{\varepsilon}_{pl} = \gamma \langle \phi(f) \rangle \frac{\partial f}{\partial \sigma}. \tag{30}$$

in which γ is a fluidity parameter depending on the viscosity of the material, $\phi(f)$ is an arbitrary function of the flow function and $\partial f/\partial \sigma$ represents the direction of the plastic flow. The notation $\langle \phi(f) \rangle$ implies that $\langle \phi(f) \rangle = 0$ if $f \leqslant 0$ and that $\langle \phi(f) \rangle = \phi(f)$ if $f > 0$.

A different approach, which in its elaboration closer connects to the rate-dependent plasticity theory, has been proposed by Duvaut and Lions and is described by Simo *et al.* (1988) and Loret and Prevost (1990). The theory is based on the difference in response between the rate-independent material and the visco-plastic material. The visco-plastic strain rate $\dot{\varepsilon}_{pl}$ and the hardening rate $\dot{\kappa}$ are defined as

$$\dot{\varepsilon}_{pl} = \frac{1}{\eta} [D_e]^{-1} (\sigma - \sigma_p) \tag{31}$$

and

$$\dot{\kappa} = -\frac{1}{\eta} (\kappa - \kappa_p), \tag{32}$$

respectively. The vector σ_p is the projection of the current stress on the yield surface and κ_p is determined by the rate-independent plastic strain history. The viscosity parameter η represents the relaxation time of the material. Equations (31) and (32) are valid if $f(\sigma, \kappa) > 0$ and if this condition is not met $\dot{\varepsilon}_{pl}$ and $\dot{\kappa}$ are both equal to zero.

A comparison can be made between the two softening visco-plastic models and the rate-dependent crack model. For the one-dimensional case and a linear softening model the yield function reduces to

$$f(\sigma, \varepsilon_{pl}) = \sigma - (\bar{\sigma}_0 + h\varepsilon_{pl}), \tag{33}$$

in which $\bar{\sigma}_0$ is the initial yield strength of the material. Substitution of $\phi(f) = f/\bar{\sigma}_0$ in the Perzyna visco-plastic model yields

$$\dot{\varepsilon}_{pl} = \frac{\gamma}{\bar{\sigma}_0} (\sigma - \bar{\sigma}_0 - h\varepsilon_{pl}). \tag{34}$$

The Duvaut–Lions model for the one-dimensional case reads

$$\dot{\varepsilon}_{pl} = \frac{1}{\eta E} (\sigma - \bar{\sigma}_0 - h\varepsilon_{pl}). \tag{35}$$

If we compare eqn (3) with (34) and (35) it is obvious that, for continued loading in a material point, the three models coincide for the one-dimensional case if

$$m = \frac{\bar{\sigma}_0}{\gamma} = \eta E. \tag{36}$$

Another type of rate dependence is used in a model formulated by Needleman (1988) and Asaro (1983). In the one-dimensional formulation of the model the plastic strain rate is chosen according to a power law function

$$\dot{\varepsilon}_{pl} = a(\sigma/g)^n, \tag{37}$$

where a is a material parameter of dimension $1/s$ and g is a hardness parameter which depends on the plastic strain. The parameter n depends on the strain rate sensitivity of the material. The distinction between this model and the rate-dependent crack model is that the strain rate is a function of the total stress (σ) and not of a part of the stress ($\sigma - \sigma_{cr}$). Instead of a parallel softening–damper element (see Fig. 1) we now only have a non-linear damper element with a power law characteristic (see Fig. 3). Needleman has used the power law formulation in a plasticity model for the investigation of shear band formation in structural metals. Here, we use it within the framework of a principal stress criterion model for the description of fracture zones in brittle materials. For the parameter g a bilinear diagram is used with an evolution law according to

$$\dot{g} = \begin{cases} H_1 \dot{\varepsilon}_{pl} & \text{for} \quad \varepsilon_{pl} \leqslant \varepsilon_{plm} \\ H_2 \dot{\varepsilon}_{pl} & \text{for} \quad \varepsilon_{pl} > \varepsilon_{plm} \end{cases} \tag{38}$$

with $g(0) = \bar{\sigma}_0$ and ε_{plm} the transition strain between hardening ($\varepsilon_{pl} < \varepsilon_{plm}$) and softening ($\varepsilon_{pl} > \varepsilon_{plm}$). In Fig. 3 computed stress-strain curves are plotted for different strain rates. Additional to the parameters of the previous model we have chosen: $a = 4.0 \text{ s}^{-1}$, $n = 50$, $\varepsilon_{plm} = \frac{1}{2}\bar{\sigma}_0/E$, $H_1 = 2500$ N mm^{-2} and $H_2 = -250$ N mm^{-2}. The implicit length scale parameter l is defined by (Needleman, 1988)

$$l = \frac{c_e}{a}, \tag{39}$$

which can be considered as the distance an elastic wave travels in a characteristic time $1/a$. If we take $n = 1$ and consider the case of softening ($H_2 < 0$) the wave equation for the Needleman model reads

$$\frac{g}{a}\left(\frac{1}{c_e^2}\frac{\partial^2 u}{\partial t^3} - \frac{\partial^3 u}{\partial x^2 \partial t}\right) + \rho \frac{\partial^2 u}{\partial t^2} = \frac{H_2}{a}\frac{\partial \varepsilon_{pl}}{\partial t}\left(\frac{\partial^2 u}{\partial x^2} - \frac{1}{c_e^2}\frac{\partial^2 u}{\partial t^2}\right). \tag{40}$$

The same third-order terms as in the wave equation for the rate-dependent bar [eqn (21)] appear, multiplied with a softening term g/a. These third-order terms, which determine the well-posedness of the solution, gradually vanish when strain softening occurs ($g(\varepsilon_{pl}) \to 0$).
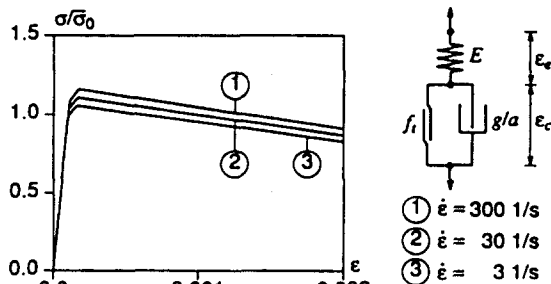

Fig. 3. Needleman's rate-dependent model for different strain rates.

Therefore, the initial value problem quickly becomes ill-posed for steep softening branches as in concrete. This means that proper results can only be obtained for ductile strain-softening models. It is furthermore noted that in this model the width of the localization zone is a decreasing function of the plastic strain.

6. NUMERICAL EXAMPLES

To investigate the performance of the rate-dependent crack model and the Needleman model numerical simulations have been carried out for a bar in uniaxial tension. The problem of mesh-sensitivity and the solution thereof can be demonstrated clearly by means of this one-dimensional problem. Attention was focused on the influence of mesh spacing on strain localization in the bar, the wave reflection on cracked zones and the consumption of energy in the cracked bar. The problem is sketched in Fig. 4: the magnitude of the impact load is taken as 75% of the maximum tensile load in the static case, whilst the loading rate is determined by time span t_d. The bar has a length of 100 mm and is divided into 10, 20, 40 and 80 elements respectively. Use has been made of eight-noded elements with a nine-point Gauss integration scheme. The longitudinal linear elastic wave speed $c_e = 1000$ m s^{-1}. If not specifically stated otherwise the material parameters are as given in Fig. 1 for the rate-dependent crack model or as given in Fig. 3 for Needleman's model. The response of the bar is linearly elastic until the loading wave reaches the left boundary where reflection of the wave causes crack initiation. The material enters the softening regime and a localization zone of intense straining emerges. The time integration of the field equations has been done with an unconditionally stable Newmark scheme ($\beta = \frac{1}{4}, \gamma = \frac{1}{2}$) (Hughes, 1987).

6.1. Rate-independent crack model

Firstly, however, analyses with a rate-independent solid have been carried out to demonstrate the mesh dependence of strain localization, wave reflection and energy dissipation. To make the analyses more instructive and avoid an almost instant failure of the bar the softening modulus is taken as $h = -1000$ N mm^{-2}. We consider a block wave with a vertical stress front which corresponds to $t_d = 0$. In Fig. 5 the results for the different meshes are plotted at a time upon which the wave returns at the point of loading. Mesh sensitivity is obvious from the strain plots: strain localization occurs at only one integration point which is the smallest possible zone. The results for the discretizations with 40 and 80 elements have not been plotted because at $t = 0.2 \cdot 10^{-3}$ s the bar has already failed. The stress plots show that the amount of wave reflection depends on the mesh: the more elements present, the larger the reduction in stress of the reflected wave. Moreover the development of the internal energy E_{int} in the bar depends on the number of elements in the mesh as can be seen from Fig. 5. In the limiting case failure can occur at $t = 0.1 \cdot 10^{-3}$ s without any further energy consumption of the bar.

6.2. Rate-dependent crack model

Rate-dependence is applied according to the constitutive equations (15)-(17). It appears that the choice $\theta = \frac{1}{2}$ for the interpolation parameter in combination with a time step $\Delta t = 5 \cdot 10^{-7}$ s gives stable and accurate results. Use of the reference material parameter set results in a length scale parameter $l = 20$ mm. The same loading pulse with $t_d = 0$ is applied. For the rate-dependent solid a localization zone emerges that converges to a finite, constant band width upon mesh refinement. In Fig. 6 the strain localization is plotted for different meshes to demonstrate the uniqueness of the solution. The exponential decrease in strain after reflection as derived in the analytical consideration in Section 4 comes out
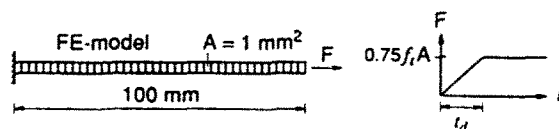

Fig. 4. Finite element model (40 elements) and time-load diagram.

(a)

ε [×10⁻³]

4.0

3.0

2.0   ← 20 elements

1.0   ← 10 elements

0.0

0.0   100
                    → x [mm]

(b)   σ [N/mm²]

2.0   80 elements

       10 elements

1.0

0.0

0.0   100
                    → x [mm]

(c)   Eᵢₙₜ [Nmm]

16   × failure

12   10 elements

8   80 elements

4   analytical
         solution
         ill-posed problem
0

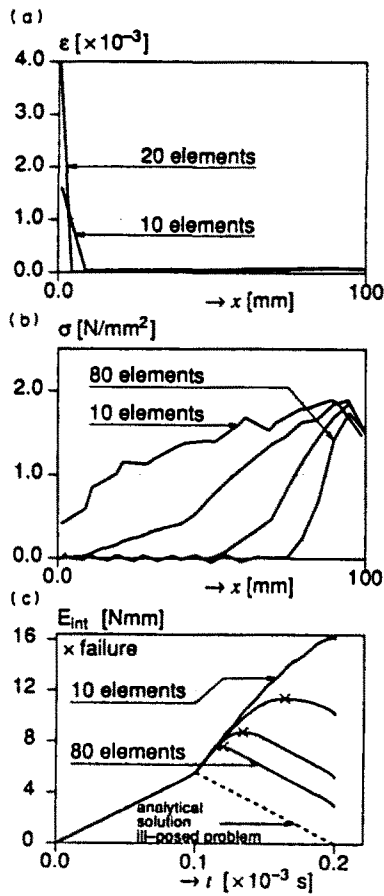0.0   0.1   0.2
            → t [×10⁻³ s]

Fig. 5. Rate-independent model with $t_d = 0$ s. (a) Strain localization along the bar at $t = 0.2 \cdot 10^{-3}$ s. (b) Stress profiles along the bar at $t = 0.2 \cdot 10^{-3}$ s. (c) Energy consumption in the bar.

(a)   (b)

ε [×10⁻³]   ε [×10⁻³]

       20, 40 and 80 elements   0.6

       10 elements   0.4

                                       0.2

                                       0.0

0.0   100   0.0   100
       → x [mm]   → x [mm]

(c)   σ [N/mm²]   (d)   Eᵢₙₜ [×10⁻³ Nmm]

                                       20

2.0   16   10 - 80 elements

                                       12

                                       8

1.0   80 elements   4

           10 elements   0

0.0
0.0   100   0.0   0.1   0.2
       → x [mm]   → t [×10⁻³ s]
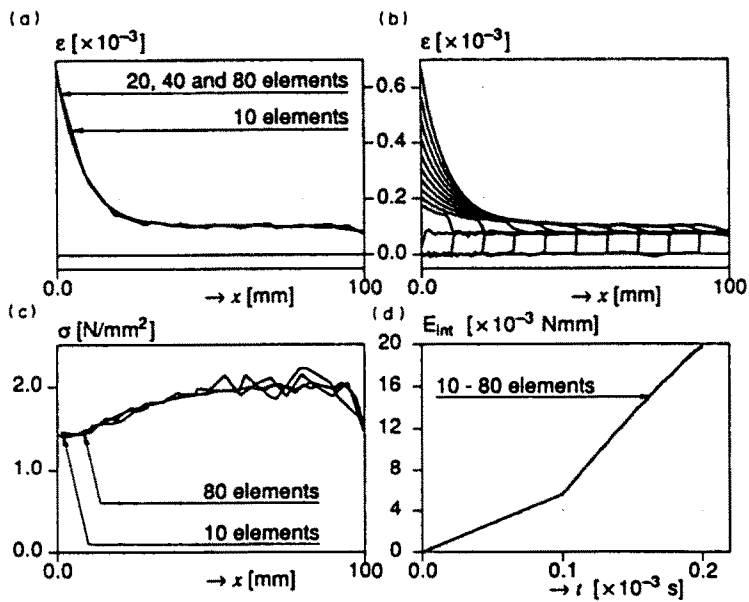
Fig. 6. Rate-dependent model with $t_d = 0$ s. (a) Strain localization along the bar at $t = 0.2 \cdot 10^{-3}$ s. (b) Development of the localization band (80 elements). (c) Stress profiles along the bar at $t = 0.2 \cdot 10^{-3}$ s. (d) Energy consumption in the bar.
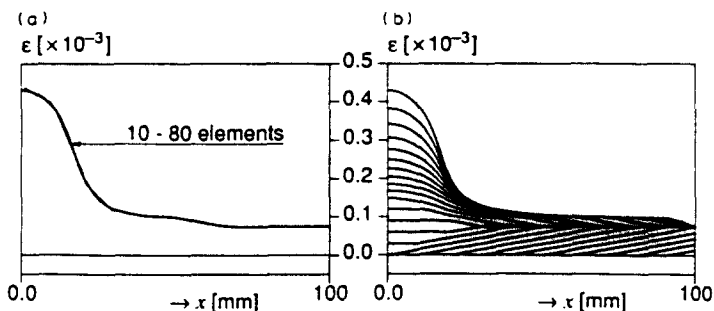
(a)
$\varepsilon\,[\times 10^{-3}]$

(b)
$\varepsilon\,[\times 10^{-3}]$

10 - 80 elements

0.5
0.4
0.3
0.2
0.1
0.0

0.0   → x [mm]   100   0.0   → x [mm]   100

Fig. 7. Rate-dependent model with $t_d = 50 \cdot 10^{-6}$ s. (a) Strain localization along the bar at
$t = 0.25 \cdot 10^{-3}$ s. (b) Development of the localization band (80 elements).

nicely. The coarse mesh (10 elements) still deviates somewhat but the fine meshes give identical results, not only in the sense that the band width is constant but also that the energy dissipation is constant during computation and the wave reflection pattern is mesh objective as can be seen from the stress profiles (Fig. 6).

A second analysis has been carried out for a different loading pulse. In the time–load diagram the time span t_d is chosen as $50 \cdot 10^{-6}$ s. So, the loading pulse firstly increases linearly in time before it becomes constant. Again the effect of the inclusion of the length scale can be observed from the strain localization plots in Fig. 7. Convergence to a unique solution with a finite localization zone characterizes the mesh independence. It is noted that the strain distribution in the localization zone has a different shape for this loading case. In the previous analysis a sharp peak in the strain occurs at the left boundary, whereas in this analysis the strain profile is more uniformly distributed and has a lower peak value. This is due to the strain rate profiles in the bar at the moment of cracking. In the previous analysis cracking is initiated at one point on the left boundary from which the exponential decay started. In this analysis the static tensile strength is exceeded over a zone with a certain length (exact length = 16.7 mm). Now, at the edge of this zone ($x = 16.7$ mm) the damping starts exponentially and at this point a bending point in the strain occurs (see Fig. 7).

Finally, the localization band width has been analysed. Firstly, the influence of the length scale parameter on the observed localization width was investigated in an analysis with $t_d = 0$ by using three different values for l, namely 15, 20 and 25 mm. From the left-hand plot of Fig. 8 it appears that the width of the localized zone is a function of the length scale parameter. These results agree with the fact that the localization zone vanishes when the length scale parameter approaches zero. A comparison of the results shown in Figs 6 and 7 had already made it clear that the shape of the loading wave influences the strain rate distribution in the localization zone and therefore also the localization band width. This effect is shown in the right-hand plot of Fig. 8 by taking three different values for the time span t_d in which the load is increased from zero to its maximum value.
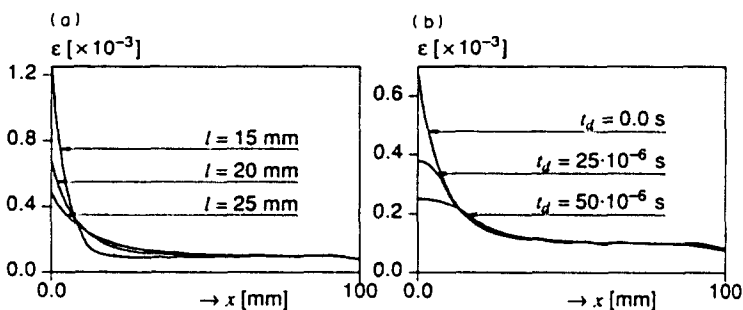
(a)
$\varepsilon\,[\times 10^{-3}]$

1.2
0.8 $l = 15$ mm
             $l = 20$ mm
0.4 $l = 25$ mm
0.0
0.0   → x [mm]   100

(b)
$\varepsilon\,[\times 10^{-3}]$

0.6 $t_d = 0.0$ s
0.4 $t_d = 25 \cdot 10^{-6}$ s
0.2 $t_d = 50 \cdot 10^{-6}$ s
0.0
0.0   → x [mm]   100

Fig. 8. (a) Variation of the length scale parameter ($t = 0.2 \cdot 10^{-3}$ s). (b) Variation of the loading rate ($t = 0.2 \cdot 10^{-3}$ s).

(a)

$\varepsilon\,[\times 10^{-3}]$

10 elements

20, 40 and 80 elements

(b)

$\varepsilon\,[\times 10^{-3}]$

-0.4
-0.3
-0.2
-0.1
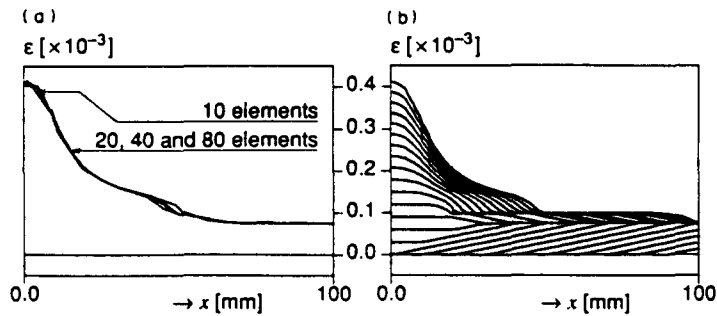-0.0

0.0 → x [mm] 100   0.0 → x [mm] 100

Fig. 9. Needleman's rate-dependent model with $t_d = 50 \cdot 10^{-6}$ s. (a) Strain localization along the bar at $t = 0.25 \cdot 10^{-3}$ s. (b) Development of the localization band (40 elements).

6.3. Needleman's rate-dependent model

We have also used the bar problem for a mesh-sensitivity analysis of Needleman's model (1988). Mesh independence has been obtained only for an analysis with a rather small negative slope ($H_2 = -250$ N mm^{-2}) and a small loading rate corresponding to a time span $t_d = 50 \cdot 10^{-6}$ s. In Fig. 9 it is shown that the localization zone is more or less constant, independent of the discretization of the bar. It appeared, however, that at a higher strain level, when the stabilizing viscous effect gradually disappears [see eqn (40)], localization again becomes mesh-dependent. This type of behaviour becomes worse when a strain-softening model with a steeper branch (more brittle) is used or when the loading rate is increased. From the right-hand plot of Fig. 9 we observe that the localization zone increases in thickness in the course of time due to the small hardening region in the model.

7. CONCLUDING REMARKS

A smeared-crack model has been proposed that includes a dependence on the strain rate. The essential features of the rate-dependent model are the implicit presence of an internal length scale and the dispersive character of wave propagation. Hence we arrive at a proper mathematical description of the softening material and we are able to simulate the localization process properly. Numerical analyses have proved the mesh objectivity of the model with respect to the width of the localization zone, the dissipation of energy and the wave reflection on the cracked zone. The width of the localization zone depends on the length scale parameter and the loading rate. The model proposed by Needleman (1988) also gives mesh-independent results but not unconditionally.

REFERENCES

Asaro, R. J. (1983). Mechanics of crystals and poly-crystals. *Adv. Appl. Mech.* 23, 2 115.
Bažant, Z. P. and Belytschko, T. B. (1985). Wave propagation in a strain softening bar—exact solution. *ASCE J. Engng Mech.* 111(3), 381 389.
Bažant, Z. P. and Oh, B. (1983). Crack band theory for fracture of concrete. *RILEM Mat. Struct.* 16, 155-177.
de Borst, R. (1990). Simulation of localization using Cosserat theory. *Proc. 2nd Int. Conf. Computer Aided Analysis and Design of Concrete Structures* (Edited by N. Bićanić and H. A. Mang), pp. 931 944. Pineridge Press, Swansea.
de Borst, R. and Mühlhaus, H.-B. (1991a). Continuum models for discontinuous media. *Proc. Conf. on Fracture Processes in Brittle Disordered Materials* (Edited by J. van Mier, J. G. Rots and A. Bakker), pp. 601-618. Chapman and Hall, London.
de Borst, R. and Mühlhaus, H.-B. (1991b). Computational strategies for gradient continuum models with a view to localization of deformation. *Proc. Int. Conf. on Nonlinear Engng Comp.* (Edited by N. Bićanić, P. Marović, D. R. J. Owen, V. Jović and A. Mihanović), pp. 239 260. Pineridge Press, Swansea.
de Borst, R. and Nauta, P. (1985). Non-orthogonal cracks in a smeared finite element model. *Engng Comput.* 2(1), 35-46.
de Borst, R. and Sluys, L. J. (1991). Localisation in a Cosserat continuum under static and dynamic loading conditions. *Comp. Meth. Appl. Mech. Engng* 90, 805-827.

Hughes, T. J. R. (1987). The finite element method—linear static and dynamic finite element analysis. Prentice-Hall, New Jersey.

Körmeling, H. A. (1986). Strain rate and temperature behaviour of steel fibre concrete in tension. Dissertation, Delft University of Technology, Delft.

Lasry, D. and Belytschko, T. B. (1988). Localization limiters in transient problems. *Int. J. Solids Structures* **24**, 581–597.

Loret, B. and Prevost, J. H. (1990). Dynamic strain localization in elasto-(visco-)plastic solids, Part 1. *Comp. Meth. Appl. Mech. Engng* **83**, 247–273.

Mühlhaus, H.-B. and Aifantis, E. C. (1991). A variational principle for gradient plasticity. *Int. J. Solids Structures* **28**, 845–858.

Mühlhaus, H.-B., de Borst, R. and Aifantis, E. C. (1991). Constitutive models and numerical analyses for inelastic materials with microstructure. *Proc. Seventh Conf. Int. Assoc. Comp. Methods and Advances in Geomechanics* (Edited by G. Beer, J. R. Booker and J. P. Carter), pp. 377–386. Balkema, Rotterdam and Boston.

Needleman, A. (1988). Material rate dependence and mesh sensitivity on localization problems. *Comp. Meth. Appl. Mech. Engng* **67**, 69–86.

Perzyna, P. (1966). Fundamental problems in viscoplasticity. In *Recent Advances in Applied Mechanics*, pp. 243–377. Academic Press, New York.

Pijaudier-Cabot, G. and Bazant, Z. P. (1987). Nonlocal damage theory. *ASCE J. Engng Mech.* **113**, 1512–1533.

Rots, J. G. (1988). Computational modeling of concrete fracture. Dissertation, Delft University of Technology, Delft.

Rots, J. G. and de Borst, R. (1989). Analysis of concrete fracture in 'direct' tension. *Int. J. Solids Structures* **25**(12), 1381–1394.

Rudnicki, J. W. and Rice, J. R. (1975). Conditions for the localization of deformation in pressure-sensitive dilatant solids. *J. Mech. Phys. Solids* **23**, 371–394.

Schreyer, H. L. and Chen, Z. (1986). One-dimensional softening with localization. *J. Appl. Mech.* **53**, 791–797.

Simo, J. C., Kennedy, J. G. and Govindjee, S. (1988). Non-smooth multisurface plasticity and viscoplasticity. Loading/unloading conditions and numerical algorithms. *Int. J. Num. Meth. Engng* **26**, 2161–2185.

Sluys, L. J. (1989). Strain softening under static and dynamic loading conditions. TU-Delft report, nr.25.2-89-5-09.

Sluys, L. J. (1992). Wave propagation, localisation and dispersion in softening solids. Dissertation, Delft University of Technology, Delft.

Sluys, L. J. and de Borst, R. (1991). Rate-dependent modelling of concrete fracture. *Heron* **36**(2), 3–15.

Sluys, L. J. and de Borst, R. (1992). Mesh-sensitivity analysis of an impact tensile test on a double-notched specimen. *Proc. 33rd U.S. Rock-Mechanics Symposium* (Edited by J. R. Tillerson and W. R. Wawersik), pp. 707–716. Balkema, Rotterdam and Boston.

Sluys, L. J., de Borst, R. and Mühlhaus, H.-B. (1991). Wave propagation and localisation in a gradient-dependent elastic plastic solid. *Proc. Int. Conf. on Nonlinear Engng Comp.* (Edited by N. Bičanić, P. Marović, D. R. J. Owen, V. Jović and A. Mihanović), pp. 287–297. Pineridge Press, Swansea.

Wu, F. H. and Freund, L. B. (1984). Deformation trapping due to thermoplastic instability in one-dimensional wave propagation. *J. Mech. Phys. Solids* **32**(2), 119–132.

Zielinski, A. J. (1982). Fracture of concrete and mortar under uniaxial impact tensile loading. Dissertation, Delft University of Technology, Delft.